RESEARCH ARTICLE

Degree of bending of concrete-filled rectangular hollow section K-joints under balanced-axial loadings

Rui ZHAO[a], Yongjian LIU[a,b*], Lei JIANG[a,b], Yisheng FU[a], Yadong ZHAO[a], Xindong ZHAO[a]

[a] *School of Highway, Chang'an University, Xi'an 710064, China*

[b] *Research Center of Highway Large Structure Engineering on Safety of Ministry of Education, Xi'an 710064, China*

[*]*Corresponding author. E-mail: liuyongjian@chd.edu.cn*

© Higher Education Press 2022

ABSTRACT   It has been found that the fatigue life of tubular joints is not only determined by the hot spot stress, but also by the stress distribution through the tube thickness represented as the degree of bending (*DoB*). Consequently, the *DoB* value should be determined to improve the accuracy of fatigue assessment for both stress-life curve and fracture mechanics methods. Currently, no *DoB* parametric formula is available for concrete-filled rectangular hollow section (CFRHS) K-joints, despite their wide use in bridge engineering. Therefore, a robust finite element (FE) analysis was carried out to calculate the *DoB* of CFRHS K-joints under balanced-axial loading. The FE model was developed and verified against a test result to ensure accuracy. A comprehensive parametric study including 190 models, was conducted to establish the relationships between the *DoB*s and four specific variables. Based on the numerical results, design equations to predict *DoB*s for CFRHS K-joints were proposed through multiple regression analysis. A reduction of 37.17% was discovered in the *DoB*, resulting in a decrease of 66.85% in the fatigue life. Inclusively, the CFRHS K-joints with same hot spot stresses, may have completely different fatigue lives due to the different *DoB*s.

KEYWORDS   fatigue assessment, K-joint, design equations, degree of bending, fracture mechanics

1 Introduction

Concrete-filled steel tubular (CFST) bridges can fully utilize material characteristics of steel and concrete, leading to an excellent structural performance and aesthetically appealing shape [1]. In China, the application of CFST truss beam bridges has become increasingly popular, with more than 400 CFST arch bridges (with a span greater than 50 m) having been built in the past 30 years. However, a significant increase in the tensile stress range in the joints is observed and is prone to fatigue failure, when considering the use of CFST truss structures from the arch system, to the beam system. Additionally, considering harsh service environment, heavy traffic loadings, and geometric defects of joints, the fatigue problem in CFST joints has become more prominent [2].

The hot spot stress (*HSS*) *S-N* curve method is the normal practice to evaluate the fatigue behavior of CFST joints, and can reflect the concentrated stress at the brace-

chord weld intersection. Xu et al. [3], Tong et al. [4], Zheng et al. [5], Musa et al. [6], Kim et al. [7], and Jiang et al. [8–13] conducted several tests and numerical studies on *HSS* of concrete-filled circular hollow section (CFCHS) and concrete-filled rectangular hollow section (CFRHS) joints. They proposed equations to predict the stress concentration factor (*SCF*). It was found that the *SCF*s were significantly decreased after concrete filling, thus prolonging the fatigue life. Li et al. [14] reported that the fatigue life of concrete-filled joints is longer than that of hollow section joints, and using the codes of hollow section joints would underestimate its fatigue life. Conversely, test studies carried out by Connolly [15], Shen and Choo [16], showed that filling the chord with concrete would shorten the fatigue life, despite the reductions in *SCF*s. The reason for this phenomenon was that the *SCF* was derived from the stress distribution on the outer wall of the tube instead of through the tube thickness. However, the latter is the key factor in determining the stress intensity factor (SIF) at the crack tip, and would control the crack growth rate at the joints

[16]. Wei et al. [17] reported that the use of SIF in fracture mechanics to evaluate the fatigue life of the joints, can effectively estimate the remaining fatigue life and has broad application prospects. Qian et al. [18] proposed that the crack propagation life of CFCHS joints accounts for 50%–90% of the total life, and should not be ignored. Thus, the influence of the through-the-thickness stress must be considered to improve the accuracy of fatigue life estimation.

The through-the-thickness stress for the location of the weld toe consists of three components: bending stress, membrane stress, and nonlinear peak stress. Among them, the nonlinear peak stress determined by the geometry of the weld, makes measurement in the design stage unrealistic [8]. In addition, it has been demonstrated that the nonlinear peak stress has little effect on the deep crack according to literature [19], so the through-the-thickness stress can be simplified to a linear combination of the bending stress, and membrane stress, as shown in Fig. 1. The degree of bending (DoB) can be used to characterize the stress distribution through the tube thickness as follows:

$$DoB = \frac{\sigma_B}{\sigma_T} = \frac{\sigma_B}{\sigma_B + \sigma_M}, \tag{1}$$

where σ_T is the total stress, σ_B is the bending stress, and σ_M is the membrane stress.

A literature review showed that numerous studies have focused on the influence of DoBs on the fatigue life. Lee and Bowness [20], Berge et al. [21], Ahmadi et al. [22−24], and Nie et al. [25], carried out tests and numerical studies on the DoB of CHS joints, and proposed the prediction equation. Shen and Choo [16] conducted numerical studies on the DoB of CFCHS T-joint and found that the DoB of CHS T-joints would decrease after filling the chord with concrete. In general, some researchers have focused on CHS and CFCHS joints, however, the understanding of the DoB on CFRHS joints is very limited despite being widely used in bridges. Compared with CFCHS joints, CFRHS joints are easy to ensure the welding quality by cutting the plates end straight [10], so better fatigue behavior can be expected.

To address this research gap, the finite elements (FE) were developed to study the DoB of CFRHS K-joints. A specimen of the CFRHS truss beam was tested to verify the FE model. A comprehensive parametric analysis was then carried out including a total of 190 FE models. This paper presents the relationships between the DoBs and four variables: brace-to-chord width ratio (β), chord width-to-thickness ratio (2γ), brace-to-chord thickness ratio (τ), and the angle between braces and chord (θ), as shown in Fig. 2. A design equation to predict the DoBs of the CFRHS K-joints was proposed using multiple regression analysis. Additionally, the maximum SCFs, and DoBs, between the CHS and CFRHS K-joints were compared. The application of the proposed DoB equation is evident in S-N curve methods and fracture mechanics methods.

2 Finite element model development and verification

2.1 Material properties

The software package ABAQUS was used to develop the FE model of CFRHS K-joints, and an elastic analysis using the experimental material properties was conducted. The chord and brace were made of grade Q345B steel. The material coupon tests were carried out
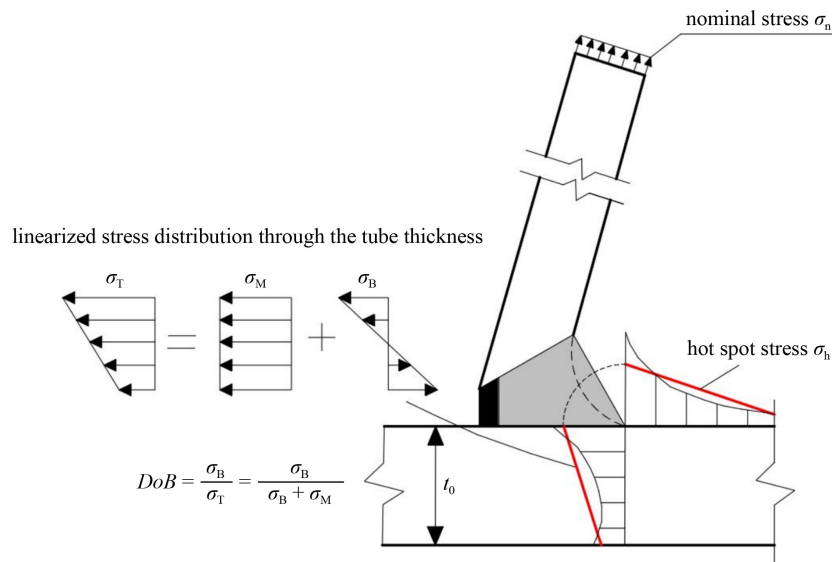

Fig. 1 Stress distribution through the chord wall thickness at weld toe.
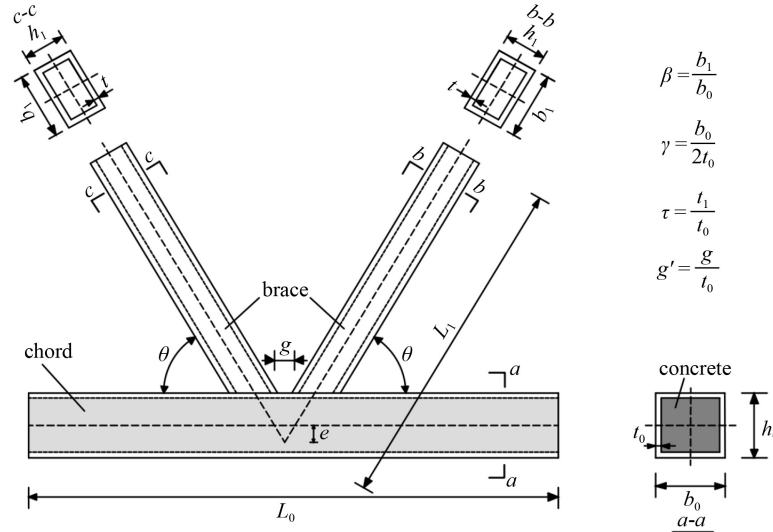
Fig. 2   Geometric parameters of the CFRHS K-joint.

according to GB/T 228.1-2010 [26]. Steel material properties are shown in Table 1, which satisfied the Chinese specification JTG D64-2015 [27]. The concrete in the chord was made of C50. The 150 mm × 150 mm × 150 mm standard specimens of concrete cube were subjected to compressive strength tests according to GB/T 50081-2002 [28]. The concrete mix ratio and material properties are shown in Table 2, which satisfied the Chinese specification JTG 3360-2018 [29]. The material properties of the joints in the FE model were based on the coupon tests.

2.2   Weld profile

It has been found that an accurate simulation of the weld profile has a significant influence on the stress field near the weld [11]. Therefore, the weld profile at the junction of the brace-chord intersection, as specified in the Chinese specification GB 50661-2011 was adopted [30]. The details of the weld profiles are presented in Table 3. As shown in Fig. 3, h_e is the weld thickness, and h_L is the weld length. b and ψ refer to the root gap, and dihedral angle between the brace and chord surface, respectively.

2.3   Element type and mesh scheme

Figure 4 shows the FE model for the CFRHS K-joint. A 20-node quadratic 3D-solid element with reduced integration (C3D20R) in the ABAQUS library was used for braces, chords, and weld profiles. To improve the calculation efficiency, only half of the model was developed considering the symmetry of the entire joint.

The structured mesh division technology in ABAQUS was adopted for mesh generation. A fine mesh with a size of approximately 1 mm was used near the intersection of brace and chord to increase the reliability of the results. To reduce the time requirement, a coarse mesh with a size of approximately 10 mm was used for regions far away from the brace-chord intersection.

A convergence test was performed before the parametric analysis to verify the FE results. A mesh sensitivity analysis determined that the layers of mesh through the tube thickness, could significantly affect the accuracy of *DoB*. The number of layers through the wall thickness should not be too small, otherwise the calculation results could be wrong or erroneous. However, the number of layers should not be too large, or it leads to a computational inefficient model. A rational layer can satisfy both the requirements of calculation accuracy and economy. Figure 5 and Table 4 show the results of the mesh sensitivity analysis with 1, 2, 3, 4, 5, and 6 layers. When the number of layers is greater than 4, the *DoB* value tend to be stable. Therefore, a four-layer mesh was selected to develop models for the consideration of computation speed.

Table 1   Steel material properties

steel plate thickness (mm)	elastic modulus E_S (GPa)	yield strength f_y (MPa)	ultimate strength f_u (MPa)	elongation (%)
4	206	425	589	28.0
6	206	414	575	29.0
8	206	445	593	28.5

Table 2   Concrete mix ratio and material properties

concrete grade	mix ratio (kg/m³)						elastic modulus E_c (GPa)	cube crushing strength f_{cu} (MPa)
	water	cement	fly ash	fine aggregate	coarse aggregate	water reducer		
C50	167	471	52	624	1109	10.46	30	56.3

Table 3 Details of the weld profile according to the GB 50661-2011 Chinese specification

parameter	detail A $\Psi = 180° - 135°$	detail B $\psi = 150° - 50°$	detail C $\psi = 75° - 30°$	detail D $\psi = 40° - 15°$
joint-included angle (α)				
max	90°	$\Psi \leqslant 105°$:60°	40°; 60° for ψ is big	—
min	45°	37.5°; 1/2ψ for ψ is small	1/2ψ	—
bevel angle of brace (ω)				
max	—	90°	determined based on the α	—
min	—	10；45° for $\Psi > 105°$	10°	—
complete weld				
h_e	$\geqslant t_b$	$\geqslant t_b$ for $\Psi \geqslant 90°$; $\geqslant \dfrac{t_b}{\sin\psi}$ for $\Psi < 90°$	$\geqslant \dfrac{t_b}{\sin\psi}$ but $\leqslant 1.75\, t_b$	$\geqslant 2t_b$
h_L	$\geqslant \dfrac{t_b}{\sin\psi}$ but $\leqslant 1.75\, t_b$	—	—	—

2.4 Steel-concrete interaction, boundary and loading conditions

As shown in Fig. 4, the mesh of the concrete and steel tubes was matched to ensure the accuracy of the calculation results, which meant that the pair of contact nodes on the interface had the exact same coordinates. The friction must also be considered for the contact point between the chords and concrete infills. Based on the literature about the steel-concrete interface [31–33], the friction coefficient ranged from 0.1 to 0.6. To consider the effect of friction on the shear force transmission under load for CFRHS K-joint, Jiang et al. [10] established a contact model with different friction coefficients. It was found that the friction coefficient of 0.3 can effectively simulate the shear between the steel-concrete interface. Therefore, the Coulomb friction model was employed with a frictional coefficient of 0.3, in this paper. In the normal direction, a "hard contact" model was employed at the steel-concrete interface, which indicated that the chord and concrete infill could not penetrate each other.

Figure 6 shows the loading and boundary conditions, of CFRHS K-joints. The balanced axial force was applied for CFRHS K-joints. Both ends of the chord were hinge-supported to ensure no bending moment existed in the chord, and ends of the two braces were applied with tension and compression with nominal stresses of 1 MPa, respectively. In this way, the extrapolated HSS has the same value with the SCF.

2.5 Determination of degree of bending values

To determine the DoB values, the bending and the membrane stresses should first be obtained, according to Eq. (1), as follows:

$$\sigma_M = \frac{\sigma_O + \sigma_I}{2}, \tag{2}$$

$$\sigma_B = \frac{\sigma_O - \sigma_I}{2}, \tag{3}$$

where, σ_O is the HSS at the outer surface, and σ_I is the HSS at the inner surface.

Based on Eqs. (1)–(3), the DoB could be further expressed as follows:

$$DoB = \frac{1}{2}\left(1 - \frac{\sigma_I}{\sigma_O}\right). \tag{4}$$

2.6 Extraction of the hot spot stress

It is recommended by IIW-XV-E [31], that the HSS of RHS joints could be derived using the quadratic extrapolation method. Three points are arranged at the location of 0.4t, 0.9t, and 1.4t away from the weld toe as specified in Table 5 and Fig. 7. In this way, the HSS could be derived as follows:

$$\sigma_h = 2.52 \cdot \sigma_{0.4t} - 2.24 \cdot \sigma_{0.9t} + 0.72 \cdot \sigma_{1.4t}. \tag{5}$$

The HSS is the stress perpendicular to the weld toe [8]. So, all the measured stresses in the extrapolated region can be modified to perpendicular as follows:

$$\sigma_\perp = \sigma_x l_1^2 + \sigma_y m_1^2 + \sigma_z n_1^2 + 2\left(\tau_{xy} l_1 m_1 + \tau_{yz} m_1 n_1 + \tau_{zx} n_1 l_1\right), \tag{6}$$

where σ_i and τ_j ($i, j = x, y, z$) are the stress components, l_1, m_1, and n_1 are vectors that can be converted to the target coordinate system.

2.7 Validation of finite element

2.7.1 Overview of the test

Until now, no test results of DoB in CFRHS K-joints are available because it is impossible to directly measure the through-the-thickness stress. However, the DoB can be derived by measuring the HSSs on the inner and outer walls of the tube according to Eq. (4). It is too difficult to arrange the strain gauges on the inner wall of the tube, in
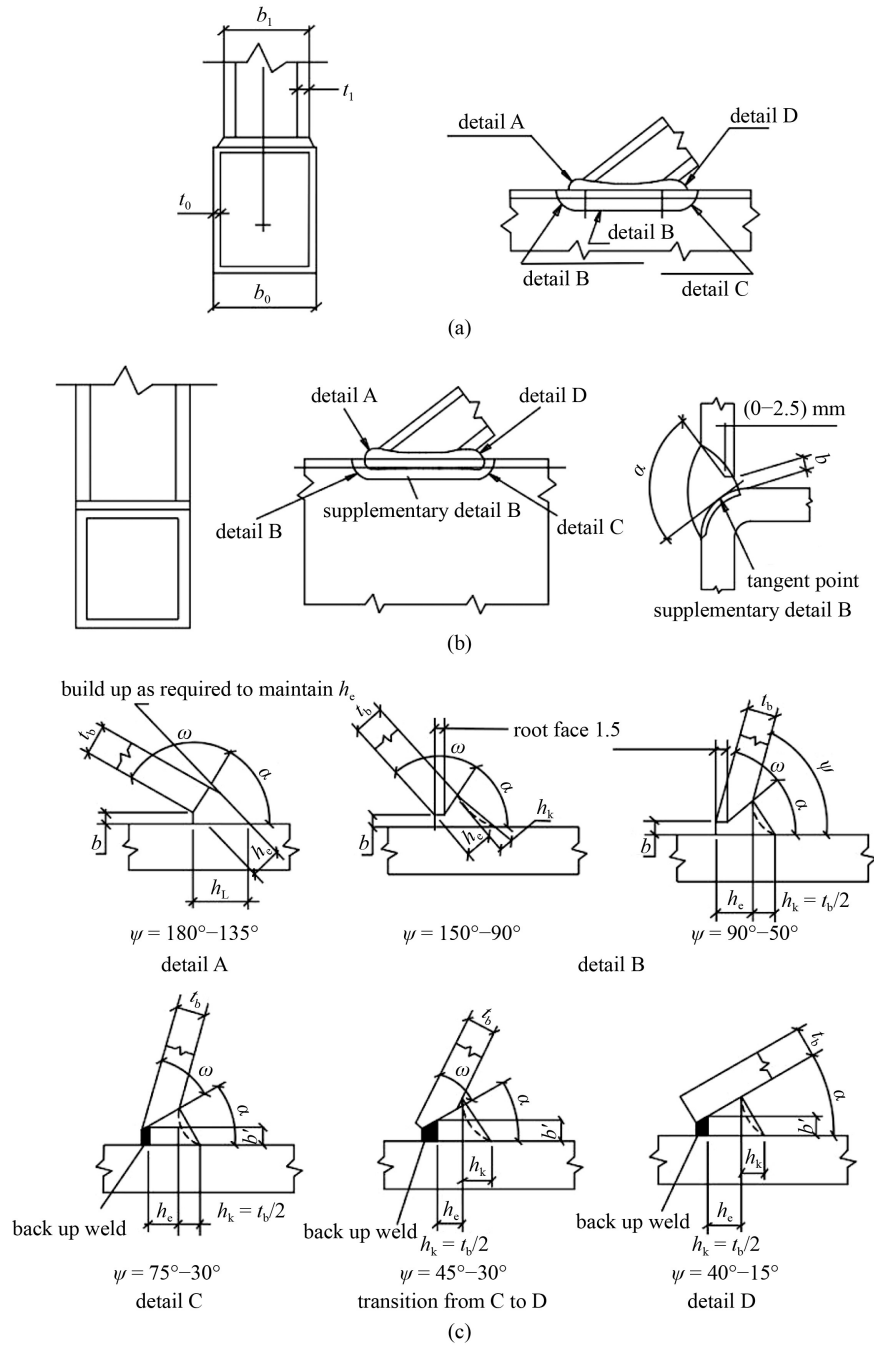
Fig. 3   Details of the weld profile in the GB 50661-2011 Chinese specification. (a) Stepped joints; (b) full-width joints; (c) welding details.

the practical sense, owing to the concrete infill. Therefore, to validate the FE models, a specimen of the CFRHS truss beam was tested and the *HSS*s on the outer wall of the tube at the brace-chord intersection were measured. Additionally, Ahmadi et al. [22–24] and Nie et al. [25] could not measure the stress on the inner wall and verified the model by the stress on the outer wall. The accuracy of the *DoB* value was ensured by controlling the number of layers through the tube thickness in Subsection 2.3.

Figures 8(a) and 8(b) show the geometry of the specimen. The span and height of the truss beam are 5.3 and 6.6 m, respectively. The upper and lower chords are both CFRHS members with cross sections of $b_0 \times h_0 \times t_0$ = 120 mm × 60 mm × 6 mm, and $b_0 \times h_0 \times t_0$ = 120 mm × 100 mm × 8 mm, respectively. The vertical and diagonal braces are RHS members with cross sections of $b_1 \times h_1 \times t_1$ = 120 mm × 80 mm × 8 mm, and $b_1 \times h_1 \times t_1$ = 120 mm × 60 mm × 6 mm, respectively. The chord and brace tubes were linked together through welds specified by GB 50661-2011 [30].

Figure 9 shows the test setup. One end of the CFRHS truss beam was fixed-supported, and the other end was movable-supported. In addition, lateral displacement limit
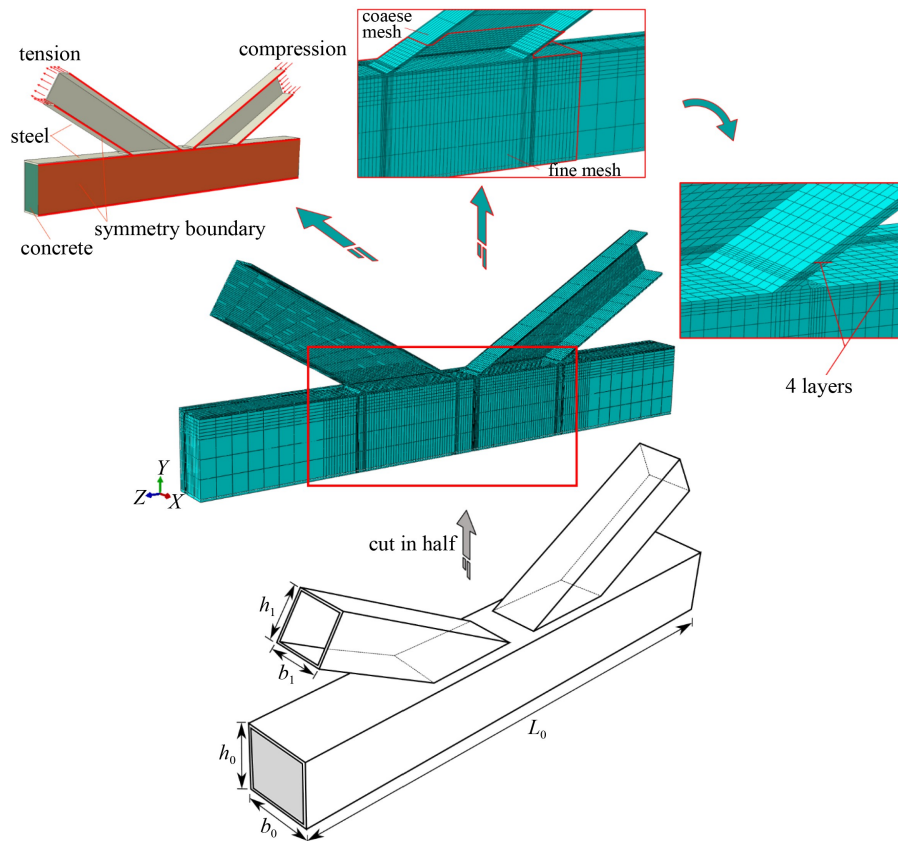
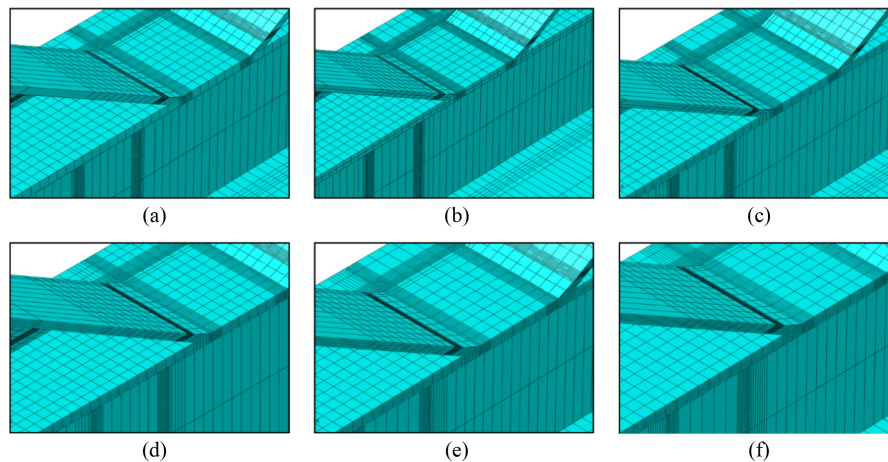**Fig. 4**   Finite element model.

Fig. 5   Density of different meshes through the tube thickness. (a) 1 layer; (b) 2 layers; (c) 3 layers; (d) 4 layers; (e) 5 layers; (f) 6 layers.

Table 4   Mesh sensitivity analysis for a typical joint ($\beta = 0.7$, $2\gamma = 30$, $\tau = 0.75$, $\theta = 30°$)

number of layers of elements through the tube thickness	DoB
1	0.8271
2	0.8448
3	0.8516
4	0.8581
5	0.8590
6	0.8592

devices were placed on both sides of the truss. A concentrated force of 100 kN was vertically applied to the middle of truss by a servo-hydraulic actuator with real-time monitoring of truss mid-span deformation through displacement meter during loading [32,33]. The CFRHS truss beam was tested twice under the same concentrated force to avoid error in the strain gauges.

Figure 8(c) shows the arrangement of the strain gauges on the outer wall of the d joint during the static tests. Lines A, B, C, D, and E are the hot spot positions specified IIW-XV-E [31] in RHS joints. The strain gauge
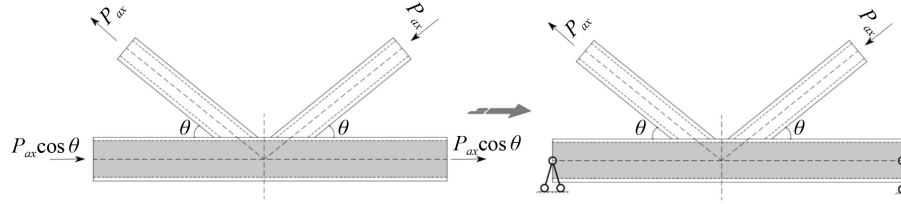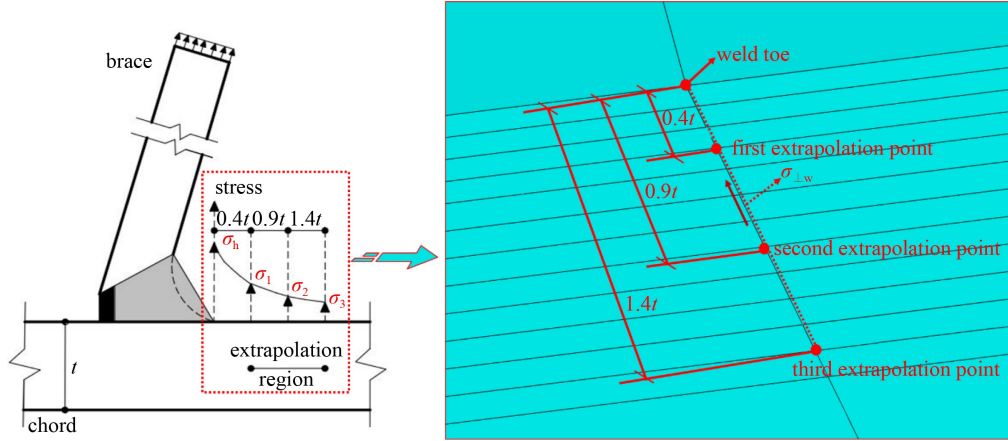
Fig. 6 Boundary and loading conditions.

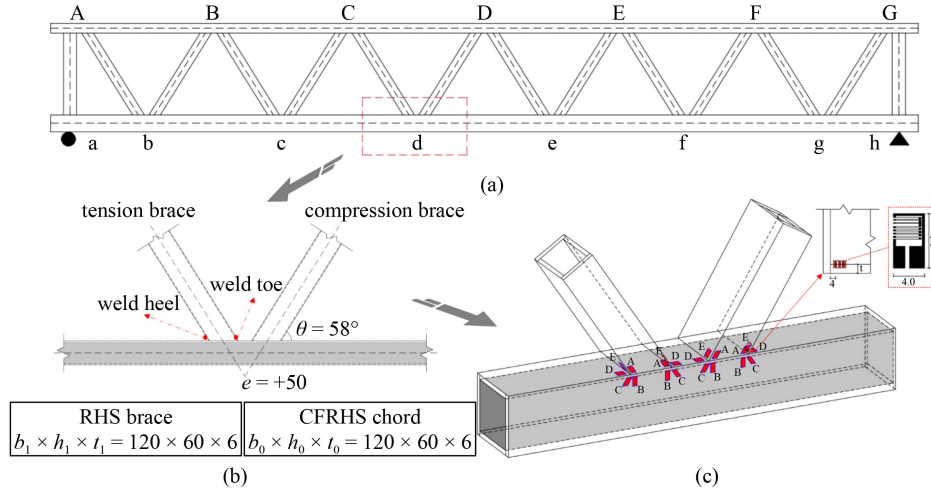**Fig. 7** Extraction of the hot spot stress.

Fig. 8 Geometry of specimen and arrangement of strain gauges (unite: mm). (a) General arrangement of truss girder; (b) test joint diagram; (c) measuring-point arrangement of *HSS*.

Table 5 The extrapolated region as recommended by IIW-XV-E

distance from weld toe	chord	brace
L_{min}	$0.4t_0$ but $\geqslant$ 4 mm	$0.4t_1$ but $\geqslant$ 4 mm
L_{max}	$L_{min} + t_0$	$L_{min} + t_1$

installed starts are 4 mm away from the weld toe and perpendicular to the weld. This satisfied the recommendation of IIW-XV-E (Table 3) [31]. Finally, the strains measured from gauges could be transformed into stresses based on the generalized Hooke's law as follows [8]:

$$\sigma = 1.1E\varepsilon. \tag{7}$$

2.7.2 Test results and finite elements verification

Figure 10(a) is the 3D solid FE model of the test truss. A fine mesh with a size of approximately 1 mm was used near the d-joint, and a coarse mesh with a size of approximately 10 mm was used for the area away from the d-joint.

Figure 10(b) shows the comparison of load-displacement curves between the FE and test results. When the load *P* is 100 kN, the truss is in the linear
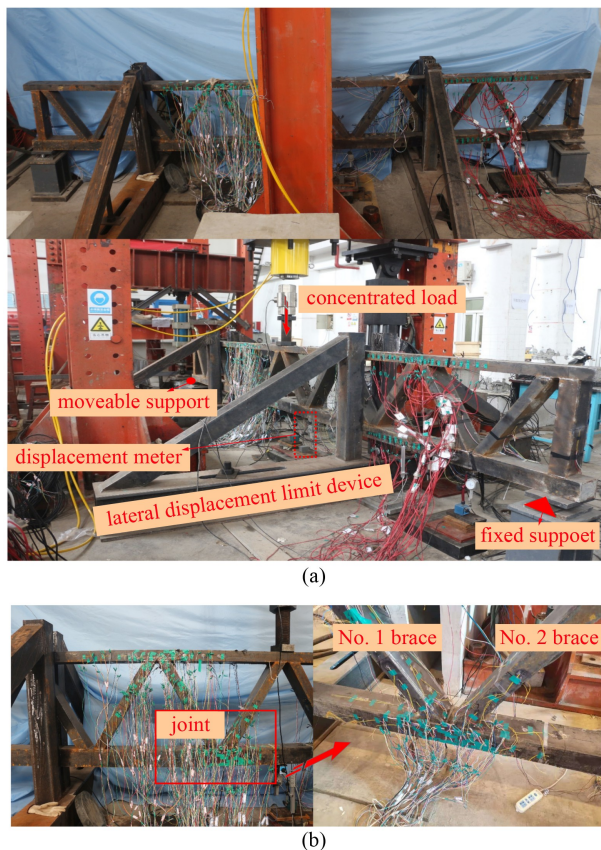
Fig. 9 Test setup. (a) General arrangement of experiment;
(b) local arrangement of experiment.

elastic stage. The FE value is consistent with the measured value, and the maximum difference is only 5%. Figure 10(c) illustrates the contrast of *HSS* between the FE and test results. It can be observed that the calculated results using the developed FE model are in clear agreement with the test results, and the average ratio of the FE to the test results is 0.98. It could be accepted that the developed FE model is reliable for calculating the *HSS*, and for predicting the *DoB* of the CFRHS joints.

3 Parametric study

3.1 Parameter design

A total of 190 models were established based on the verified FE models to evaluate the influence of geometric parameters on the *DoB* of CFRHS K-joints under a balanced axial force. According to the CIDECT guidelines, the non-dimensional geometric parameters are within the following ranges: $0.4 \leqslant \beta \leqslant 1$; $0.25 \leqslant \tau \leqslant 1$; $10 \leqslant 2\gamma \leqslant 35$; $30° \leqslant \theta \leqslant 60°$. The specific parameters are listed in Table 6. The following assumptions were made.

1) The center lines of the two braces intersect the chord center line without geometric eccentricity of the joints ($e = 0$).

2) The lengths of two braces are equal.

3) The angles between the two braces and chord are equal ($\theta_1 = \theta_2$).

4) without considering the influence of tube height-to-width ratio (h/b) on *DoB*, thus the chord is assumed to be a square section.

5) The gap joints ($g' > 0$) are normally adopted in bridge engineering. Therefore, overlapped joints ($g' < 0$) are not considered.

6) The width b_1 of the brace is the dimension along the transverse direction of the joint, that is, the x coordinate direction in Fig. 4.

The geometric dimensions of the joints were based on the CFRHS joint of the Huang-Yan Bridge [8] in China. The width and height of the chord were both 400 mm, the thickness of the chord ranged from 11 to 20 mm, the width and height of the brace ranged from 160 to 400 mm, and the thickness of the brace ranged from 3 to 40 mm. The length of the brace was 1500 mm. To eliminate the influence of end restraints on stress distributions at the brace-chord intersection according to the Saint Vernet principle, the length of the brace should be greater than 6 times the chord diameter. Therefore, the length of the chord was set to 3000 mm. For certain parameter designs, there were overlapping joints ($g' < 0$) with the following parameters: $\beta = 0.55$, $2\gamma = 35$, $\tau = 0.5$, $\theta = 60°$, $g = -23$, which are mutually exclusive to the assumed conditions, so they were ignored. Thus, there were 190 effective models exclusive of the joints that did not satisfy the assumptions mentioned above.

3.2 Extraction of degrees of bending from the finite element model

A typical model was selected to present the steps of *DoB* extraction. Firstly, the stress field of joints was obtained, and the *HSS*s at the side of weld toes and weld heels were extracted. Figure 11 shows the stress diagram for the CFRHS K-joint ($\beta = 0.4$, $2\gamma = 10$, $\tau = 0.75$, $\theta = 45°$) under a balanced axial force. Secondly, the location to extract the *DoB* was determined. The position of the maximum *HSS* (HSS_{max}) is vital for accurate fatigue assessment [20], as it presents the most likely location for fatigue failure occurrence. Therefore, this study only analyzed the *DoB* at the HSS_{max} point. Finally, the *DoB* was calculated in combination with Eq. (4) in Subsection 2.5. Figure 11 shows the distribution of *HSS* at the weld toe and weld heel of the joint. The HSS_{max} point was located at the D point of the weld toe in the tensile brace, so *DoB* = 0.88 of D point was extracted as the analysis data.

However, the location of HSS_{max} was affected by the change of joint geometric parameters. The fatigue life predictions were commonly connected with cracks in the chord member, and the HSS_{max} always occurred on the

(a)

(b)

(c)
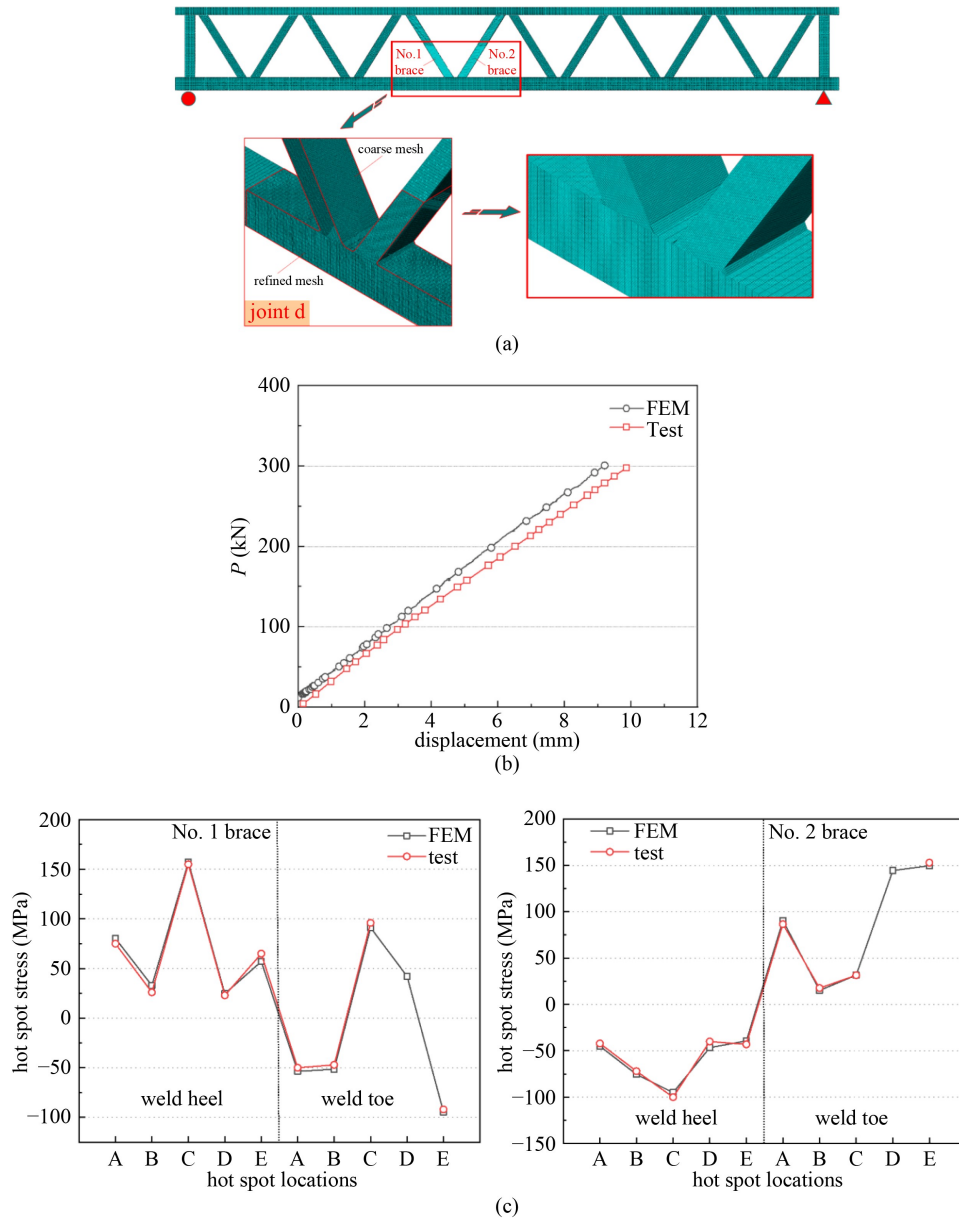
Fig. 10   FE modeling and verification. (a) FE model of the truss; (b) comparison of Load-Displacement curve between FE results and test results; (c) comparison of *HSS* between FE results and test results.

Table 6   Specific parameters for parametric analysis

parameter	values
β	0.4, 0.55, 0.7, 0.85, 1
2γ	10, 15, 20, 25, 30, 35
τ	0.25, 0.5, 0.75, 1
θ	30°, 45°, 60°

chord [34]. To provide an accurate prediction of *DoB* on the chord, this study only analyzed Lines B, C, and D. Figure 12 shows the influence of four variables on the HSS_{max} location. As shown in Fig. 12(a), with the increase of β, the proportion of HSS_{max} at point D increases, while that at point C decreases. When $\beta = 0.85$, there is almost no HSS_{max} at point C. As shown in Fig. 12(b),

with the increase of 2γ, the proportion of HSS_{max} at point C increases, while that at point B decreases. As shown in Fig. 12(c), the proportion of HSS_{max} at point B increases, and that at point C decreases with the increase of τ. As shown in Fig. 12(d), with the increase of θ, the proportion of HSS_{max} at point C increases, while those at points B and D decrease. In addition, the HSS_{max} at points B and D are almost equal in proportion to the change of θ.

3.3   Effects of the concrete on degrees of bending

To evaluate the influence of concrete on *DoB*, Fig. 13 shows the comparison of *DoB* between CFRHS and RHS K-joint in the parametric case of $\beta = 0.4$, $2\gamma = 10$, $\tau = 0.75$, and $\theta = 45°$. It can be found that after filling the

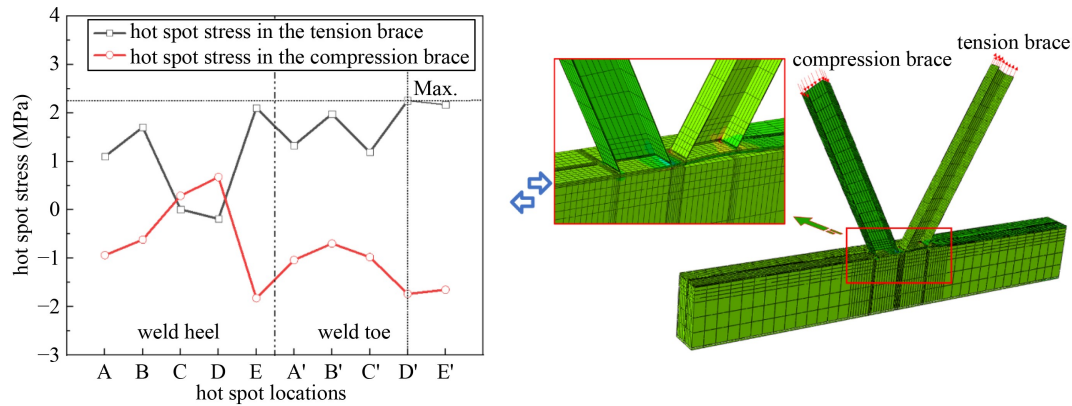**Fig. 11** The *HSS* distribution ($\beta = 0.4$, $2\gamma = 10$, $\tau = 0.75$, $\theta = 45°$).

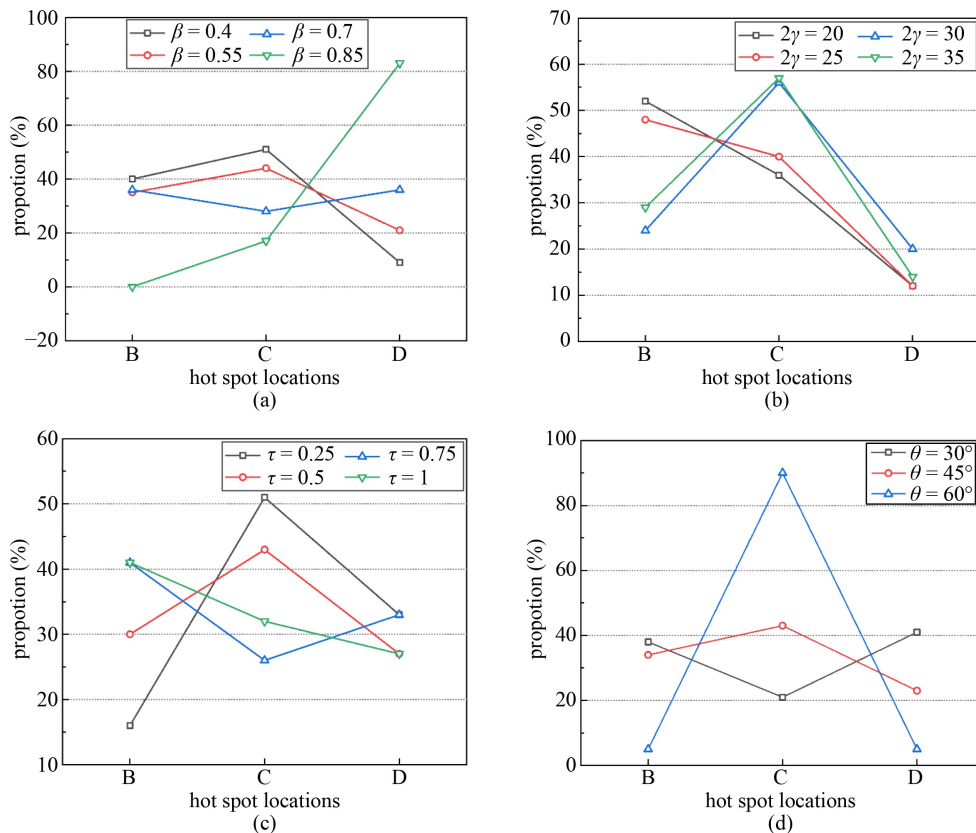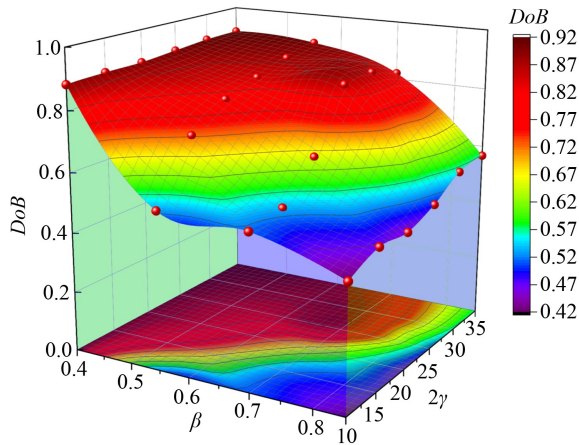**Fig. 12** Influence of four variables on hot spot location (a) β; (b) 2γ; (c) τ; (d) θ.

chord with concrete, σ_O, σ_I, and σ_M decreases, however, the *DoB* increases. For tubular joints with a defect, a higher *DoB* is related to a smaller crack driving force, which means that the fatigue performance of RHS joints is improved after filling the chord with concrete. As shown in Fig. 11, the deformation of the tension brace was greater than that of the compression brace. The reason for this phenomenon is that the infilled concrete significantly limits the vertical deformation of the brace under compression, but the brace under tension is less restricted. The action of concrete leads to the redistribution of three-dimensional stress field of joints, making it necessary to study the *DoB* of the joints after concrete filling.

3.4 Effects of β on degrees of bending

Figure 14 shows the effects of β on *DoB*s. The figure was drawn by varying β ratios ($\beta = 0.4$, 0.55, 0.7, and 0.85) and keeping τ and θ ratios constant ($\tau = 0.25$, $\theta = 30°$). It can be found that with the increase of β, *DoB* decreases, which indicates that β has significant effect on *DoB*. Also, the downward trend of *DoB* slows down with the increase of 2γ under constant β. As β increases, the width of the chord decreases, resulting in a smaller cross-sectional area of the chord. Therefore, the membrane stress per unit area of the cross section of the chord becomes larger, resulting in a higher ratio of membrane
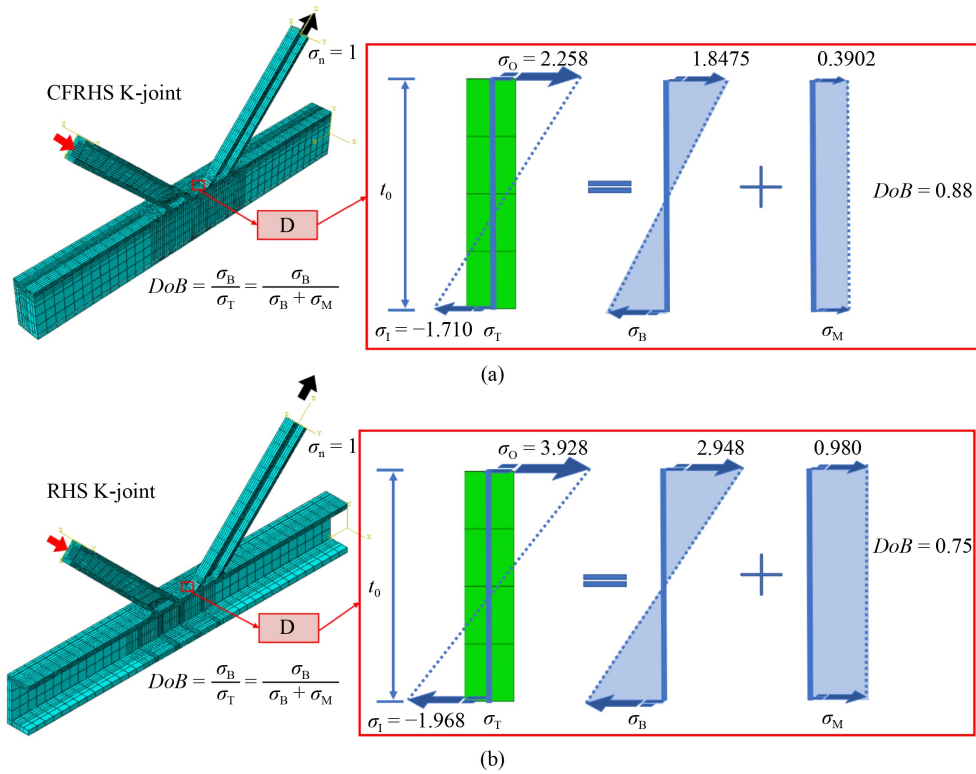
Fig. 13   A comparison of the DOB_{CFRHS} and DOB_{CHS} ($\beta = 0.4$, $2\gamma = 10$, $\tau = 0.75$, $\theta = 45°$). (a) CFRHS K-joint; (b) RHS K-joint.

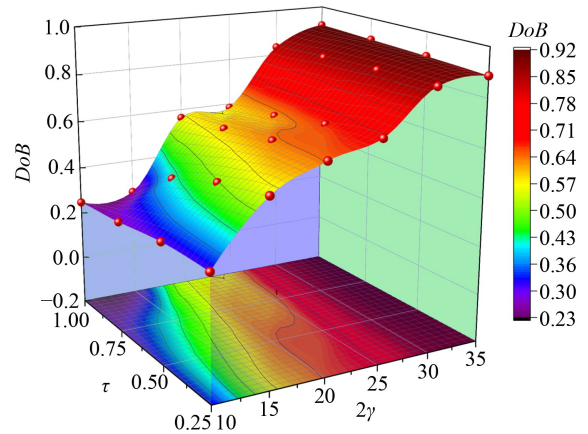Fig. 14   Influence of β on the *DoB* under balanced axial force ($\tau = 0.25$, $\theta = 30°$).

Fig. 15   Influence of γ on the *DoB* under balanced axial force ($\beta = 0.7$, $\theta = 45°$).

stress to the total stress. It is demonstrated that a wider chord will lead to a lower value of *DoB*, which can also be explained in the fact that the axis and rotational stiffness of the chord increase with decreasing β ratios, which brings about higher bending stress due to balanced axial force.

3.5   Effects of γ on degrees of bending

Figure 15 shows the influence of parameter γ on the *DoB* under a balanced axial force. The figure was drawn by varying 2γ ratios ($2\gamma = 10$, 15, 20, 25, and 30) and keeping θ and β constant ($\beta = 0.7$, $\theta = 45°$). The *DoB* increases with an increase in 2γ. Changes in the *DoB* were also significantly affected by 2γ. This indicates that the thickness of the chord has a significant effect on the *DoB* under constant chord width. With the increase of γ, the chord width increases, resulting in a larger cross section area of the chord. Thus, the membrane stress per unit area of the main cross section becomes smaller, resulting in a lower ratio of membrane stress to total stress. Furthermore, the wider the chord width, the greater the value of *DoB*. It is also attributed to the chord filling with concrete which makes the stress distribution of the chord more uniform for lower 2γ ratios.

3.6 Effects of τ on degrees of bending

Figure 16 depicts the influence of the parameter τ on the *DoB* under a balanced axial force. The figure was presented by varying τ ratios ($\tau = 0.25, 0.5, 0.75$, and 1) and keeping θ and 2γ constant ($\theta = 30°$, $2\gamma = 30$). For a balanced axial force, the *DoB* decreases with an increase in τ. As τ increases, the chord thickness decreases, resulting in a smaller cross section area of the chord. Thus, the membrane stress per unit area of the chord cross section becomes larger, resulting in a higher ratio of membrane stress to total stress. It is demonstrated that a thinner chord will lead to a lower value of *DoB*. This also can be explained that the axis and rotational stiffness of the chord decreased with increasing τ ratios, which contributes to a smaller bending stress.

3.7 Effects of θ on degrees of bending

Figure 17 presents the influence of parameter θ on the *DoB* under a balanced axial force. The figure was plotted by changing the θ ($\theta = 30°, 45°$, and $60°$) and keeping β and τ ratios constant ($\beta = 0.4$, $\tau = 1$). The *DoB* increases gradually with an increase in θ. The results show that the value of *DoB* fluctuates less with the change in parameter θ. Both the horizontal and vertical components of the axial force of the brace contribute to the distribution of the chord wall thickness stress field. As θ increases, the vertical force component becomes larger, and the horizontal force component becomes smaller. Therefore, the effects of θ on *DoB*s can be ignored due to the contribution of the horizontal and vertical component of the axial force to the bending stress would cancel each other out.

4 Design equations to prediction degrees of bending of CFRHS K-joints

4.1 Parametric equations

Considering design, the parametric equation to predict *DoB*s for CFRHS K-joints was proposed by using multiple regression analysis. Limited number of general equations are available for fitting. However, two fitting choices are available, namely Fourier expressions and polynomials. The latter is more consistent with the FE results, easier to design, and more consistent with existing equations. Therefore, the general equation of *DoB*s was selected based on previous studies [20] for CHS K-joints as follows:

$$DoB = c_1(c_2 + c_3\beta - c_4\beta\gamma)\beta^{c_5}(2\gamma)^{c_6}\tau^{c_7}\sin^{c_8}\theta(g')^{c_9}$$
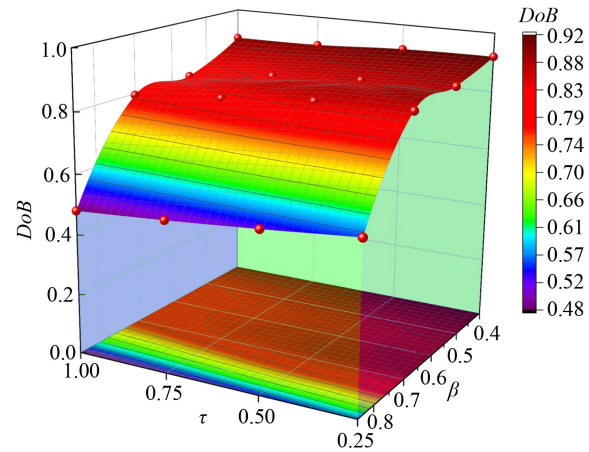$$\cdot(c_{10} + c_{11}\beta^{c_{12}}g'^{c_{13}}), \tag{8}$$

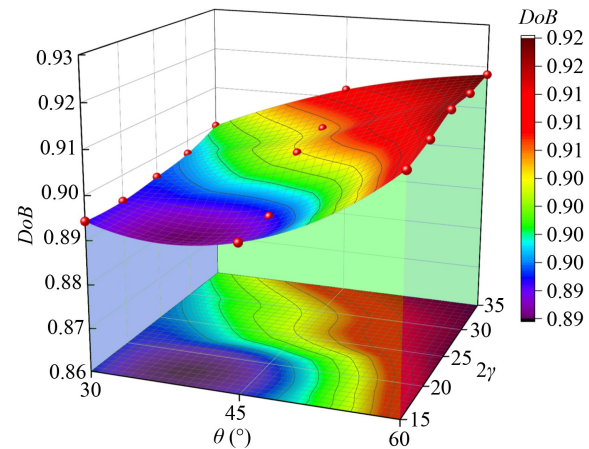**Fig. 16** Influence of τ on the *DoB* under balanced axial force ($2\gamma = 30$, $\theta = 30°$).

Fig. 17 Influence of θ on the *DoB* under balanced axial force ($\beta = 0.4$, $\tau = 1$).

where constants c_1 to c_{13} should be determined by regression analysis.

Several trials have been done to make the calculated results in agreement with the FE results, and the *DoB* parametric equation can be expressed as follows:

$$DoB = (0.80549 - 1.17278\beta + 1.15409\beta^2)(2\gamma)^{0.03701}$$
$$\cdot(1.35404 + 0.048884\tau - 0.04372\tau^2)$$
$$\cdot\sin^{0.92119}\theta(g')^{0.24689}, \ R^2 = 0.955. \tag{9}$$

The value of R^2 was quite high, therefore, Eq. (9) satisfied accuracy requirements.

4.2 Assessment of the parametric equation

To evaluate the *DoB* parametric Eq. (9), the method described by Shao and Lie [35] was used. The relative error between the *DoB* values extracted from the FE analysis and Eq. (9) was shown as follows:

$$e = \frac{DoB_P - DoB_R}{DoB_R} \times 100\%, \tag{10}$$

where, e is the relative error, DoB_P and DoB_R are *DoB*s predicted from the parametric equation and FE analysis, respectively. Figure 18 shows the relative errors for all 190 models. It can be found that all values of e are less than 5%, which indicates a good agreement between DoB_P and DoB_R.

The United Kingdom Department of Energy (DoE) [36] also suggested the judgment criteria for evaluating the accuracy of proposed equations. If (% $P/R < 1.0$) ≤ 25% and (% $P/R < 0.8$) ≤ 5%, it can be considered that the parametric equation can be accepted. P is the predicted *DoB* from the parametric equation and R is the extracted *DoB* from FE or *HSS* test. In Eq. (9), the (% $P/R < 1.0$) and (% $P/R < 0.8$) are 2.3% and 0%, which satisfies the above judgment criteria. It can be derived that Eq. (9) is accepted. In addition, the corresponding *COV* is 0.061, and the mean value of DoB_P-to-DoB_R is 1.002, which confirms a high reliability and accuracy of the parametric equation.

Although Eq. (9) is accepted, there are some value points below the line of $Y = X$, shown in Fig. 18. This is understood as the predicted result, which is overestimated. The joints with a smaller *DoB* have a larger membrane stress through the wall thickness, which is considered dangerous. The predicted value of *DoB* when less than the extracted value, by the actual FE analysis, implies that the prediction of the residual fatigue life is conservative [23]. A lower-bound value, when derived from the mean minus three times the standard deviation is ensured, and 99.73% of the data is guaranteed to be within the safe range, the parametric equation can be considered conservative. The correction factor f is proposed as follows:

$$f = \frac{DoB_D}{DoB_P}, \tag{11}$$

where DoB_D is the design value of the *DoB* predicted from the final parametric equation.

It can be concluded that the correction factor f was 0.95. The final parametric equation for prediction the *DoB* of CFRHS K-joints can be expressed as follows:

$$DoB_D = 0.95 \times DoB, \tag{12}$$

$$\begin{aligned}DoB_D = &0.92(0.80549 - 1.17278\beta + 1.15409\beta^2) \\ &\cdot (2\gamma)^{0.03701}(1.35404 + 0.048884\tau - 0.04372\tau^2) \\ &\cdot \sin^{0.92119}\theta(g')^{0.24689}.\end{aligned} \tag{13}$$

To Eq. (13), the (% $P/R < 1.0$) = 10% and (% $P/R <$

0.8) = 1.5% satisfies the above judgment criteria. Therefore, Eq. (13) is accepted.

4.3 Comparison of degrees of bending between CFRHS K-joints and CHS K-Joints

The effect of the concrete on fatigue behavior was further evaluated by a comparison of CFHS joints and hollow section (HS) joints. Up until now, only *SCF*s and *DoB*s research has been completed for CFRHS and CHS K-joints. Morgan and Lee [34] provided the parametric equations for SCF_{max} and *DoB* for CHS K-joints. Jiang et al. [10] provided the parametric equations for the SCF_{max} for CFRHS K-joints. Therefore, a comparison of the CFRHS and CHS K-joints was made based on the parameters shown in Table 6.

Figure 19 shows the comparison of the SCF_{max} values between CHS and CFRHS K-joints under a balanced-axial force. The mean value of the SCF_{CFRHS}-to-SCF_{CHS} is 2.011. This indicates an increase of 101.1% in SCF_{max} for CFRHS K-joints, compared to CHS K-joints. Figure 20 shows the comparison of *DoB* values between the CHS and CFRHS K-joints under a balanced-axial force. The mean value of the DoB_{CFRHS}-to-DoB_{CHS} is 0.944.
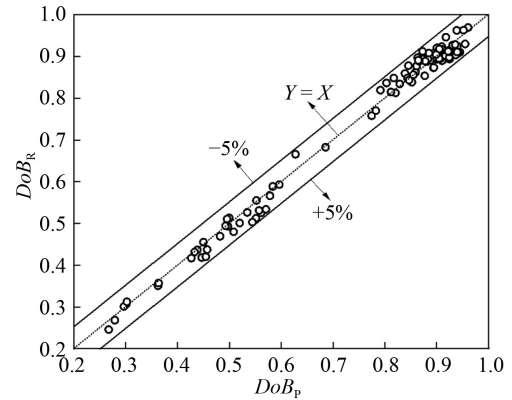
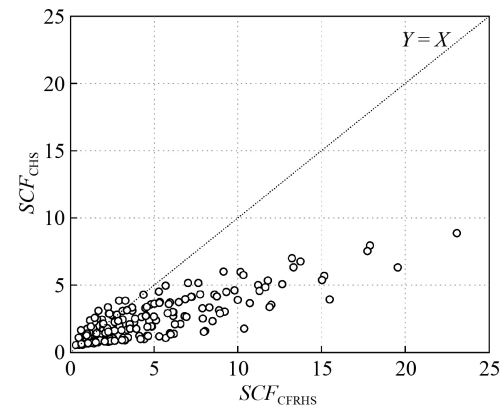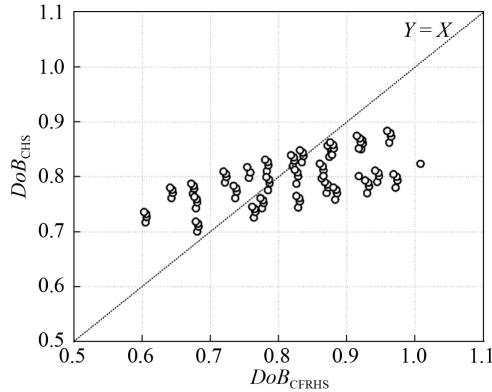**Fig. 18** Error analysis of the *DoB*s.

Fig. 19 A comparison of SCF_{CFRHS} and SCF_{CHS}.

Fig. 20 A comparison of DoB_{CFRHS} and DoB_{CHS}.

This indicates a 6.4% reduction in *DoB* for CFRHS K-joints, compared to CHS K-joints. This relationship may be due to the influence of the concrete core, which increases the stiffness of the chord and restricts the deformation of the chord tubular shape, leading to more bending stress.

Additionally, a reduction of 3.1% in *DoB* and 101.1% growth of *SCF* for CFRHS K-joints, compared to CHS K-joints, are seen. Therefore, using only *SCF* to evaluate the fatigue behavior without considering the influence of the *DoB* would result in errors.

5 Application of degree of bending

The application of the proposed *DoB* equation, improves the accuracy of the commonly used fatigue assessment in S-N curve methods and fracture mechanics methods.

5.1 *S-N* curve method

The *HSS S-N* curve method uses *SCF* as the main variable to evaluate the fatigue details, but it does not consider the through-the-thickness stress. To improve the $S-N$ curve of *HSS* accuracy, a correction factor can be introduced to solve the problem of low *DoB* results leading to unsafe evaluation of fatigue life. When the *DoB* of the joint is lower than the critical value DoB_0, the result of the fatigue life determined by the *HSS* $S-N$ curve is corrected, and the modified formula is as follows:

$$N = N_0 \left(\frac{DoB}{DoB_0} \right)^{\alpha}, \tag{14}$$

where *DoB* is the predicted values by Eq. (13). N_0 is the fatigue life obtained by the *S-N* curve method of *HSS*, and *N* is the revised value considering the stress distribution through the tube wall thickness. The α and DoB_0 were determined experimentally and were related to the geometry and material of the joint and weld.

5.2 Fracture mechanics method

In bridge engineering, the fatigue of weld joints in fatigue detail, is usually high cycle fatigue whose stress is mainly linear elastic. Therefore, this paper proposes a fatigue assessment process for weld joints based on linear elastic fracture mechanics, which can be divided as follows.

1) The stress amplitudes of the weld joints are calculated according to the geometry and load of the weld joints. The initial crack depth a_0, and crack length c_0, as well as the crack depth limits a_c, and crack length limits c_c, were given as input conditions.

2) The SIF and the SIF ranges ΔK are calculated.

In the linear elastic fracture mechanics assessment process, the residual fatigue life of the cracked joint was evaluated according to the SIF at the crack tip, which controls the rate of crack growth. The commonly used crack propagation law, is the Paris' law [37]:

$$\frac{da}{dN} = C(\Delta K)^m, \tag{15}$$

where according to Aaghaakouchak et al. [38], ΔK can be expressed as follows:

$$\Delta K = \Delta \sigma_h \left[Mk_m Y_m (1 - DoB) + Mk_b Y_b DoB (1 - a/t) \right] \sqrt{\pi a}, \tag{16}$$

where, *C* and *m* are the material constants. Mk_m and Mk_b are the weld-toe magnification factors corresponding to σ_M and σ_B, respectively. Y_m and Y_b are the plain plate shape factors corresponding to σ_M and σ_B, respectively.

3) The size of the crack-tip propagation step is calculated.

The appropriate crack depth propagation step size Δa_i is selected, which is generally advisable for $\Delta a_i = 0.1 a_{i-1}$. The smaller the propagation step size, the longer the calculation time. The propagation step if too large, results in a large error in the calculation of crack propagation.

According to Paris' law, the load cycles corresponding to all points on the crack surface of the same propagation step, are equal. Δc is be calculated as follows:

$$\Delta c = \Delta a \left(\frac{\Delta K_c}{\Delta K_a} \right)^m. \tag{17}$$

The crack depth a_i and crack length c_i is calculated as follows:

$$a_i = a_0 + \Delta a_i, \tag{18}$$

$$c_i = c_0 + \Delta c_i. \tag{19}$$

4) Determine whether the crack expands according to the decision conditions. When the decision conditions are satisfied, the crack continues to expand. Otherwise, crack propagation terminates.

The decision conditions are

$$\Delta K > K_{th}, \tag{20}$$

where K_{th} is the threshold value of fatigue crack propagation, and its value is related to the component material.

The crack shape should also be satisfied as follows:

$$a_i \leqslant a_c \ or \ c_i \leqslant c_c, \tag{21}$$

5) Remaining life predictions. According to Paris' law [37], the fatigue life is calculated as follows:

$$N = \int_{a_0}^{a_f} \frac{1}{C(\Delta K)^m} da, \tag{22}$$

where a_f is final crack depth.

Figure 21 shows a summary of the fatigue life prediction process of weld joints based on the fracture mechanics method.

5.3 Remaining fatigue life prediction of CFRHS K-joints

The remaining fatigue life of the CFRHS K-joints was predicted according to Fig. 21. A three-dimensional stress field near the brace-chord intersection was obtained by the combination of the *SCF* equations along the tube outer wall, given by Jiang et al. [10], and the *DoB* equation through the tube thickness presented in this paper. The remaining life prediction of CFRHS K-joints under a balanced-axial force theory put the data in Table 7 into practice. The remaining fatigue life can be calculated as follows:

$$N = \sum_{i=1}^{n} \Delta N_i = \frac{1}{C} \sum_{i=1}^{n} \left(\frac{\Delta a_i}{(\Delta K)_i^m} \right), \tag{23}$$

where the number of sub steps for crack propagation analysis represented symbolically by i, Δa_i is the increment of crack propagation, and ΔN_i is the crack propagation life corresponding to Δa_i.

Table 8 shows the remaining fatigue life prediction of the CFRHS K-joints with initial cracks under a balanced axial force. The *SCF*s of joint 2 and joint 1 are similar, but the *DoB* difference is 0.29, and the residual fatigue life difference is 1.583 million cycles. Additionally, a reduction of 37.17% was found in the *DoB*, resulting in a
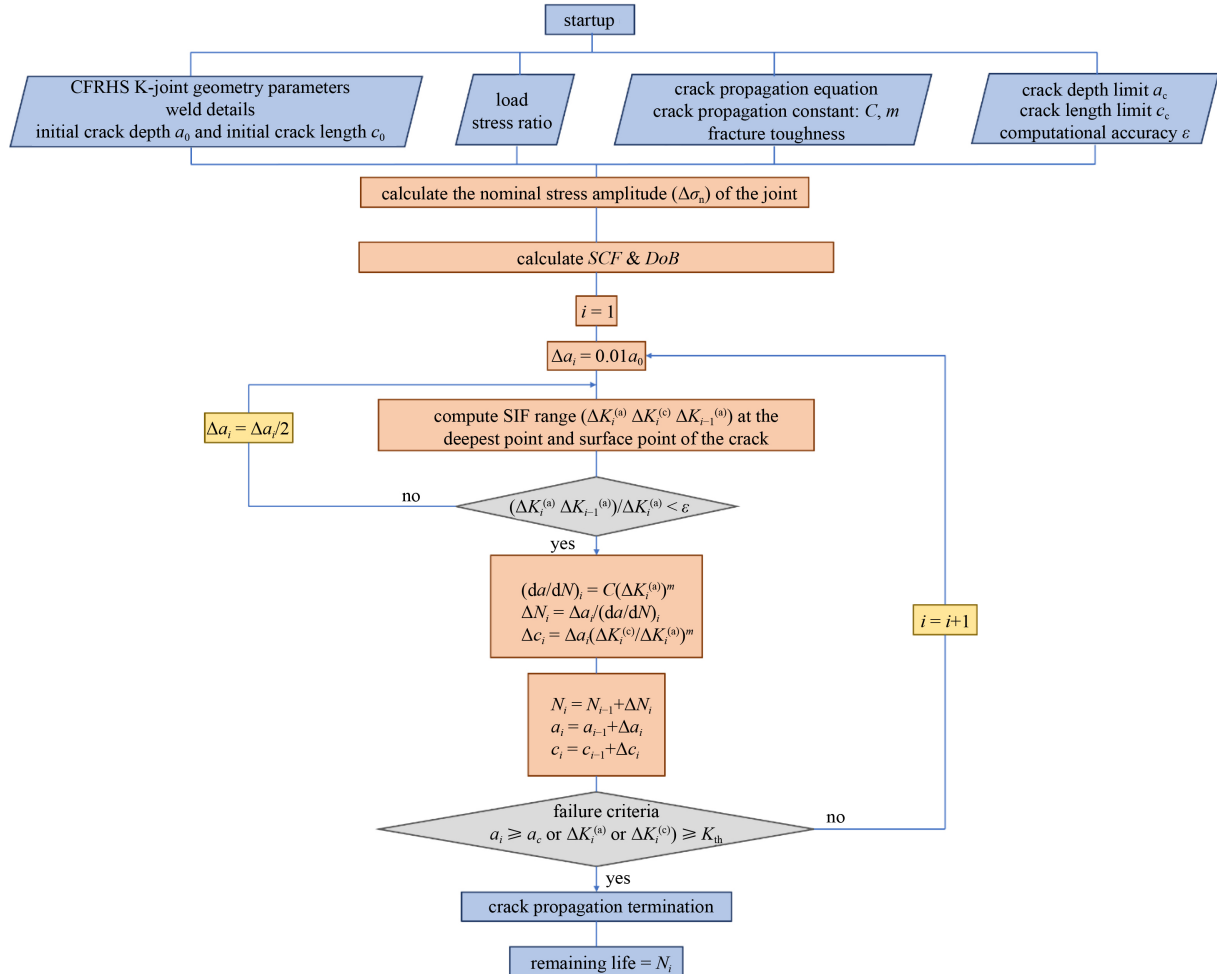

Fig. 21 Remaining life prediction process for CFRHS K-joints based on fracture mechanics.

Table 7 Input parameters used for remaining fatigue life prediction of CFRHS K-joints

input parameters	joint	
	joint 1	joint 2
chord length L_0	3000 mm	3000 mm
chord width b_0	400 mm	400 mm
chord height h_0	400 mm	400 mm
chord thickness t_0	27 mm	13 mm
brace length L_1	1500 mm	1500 mm
brace width b_1	160 mm	340 mm
brace height h_1	160 mm	340 mm
brace thickness t_1	13 mm	3 mm
brace inclination θ	30°	30°
axial load	$10000N$	$10000N$
fracture toughness	63 N·mm$^{-3/2}$	63 N·mm$^{-3/2}$
crack growth equation	Paris	Paris
C	5.21×10^{-13} N·mm$^{-3/2}$	5.21×10^{-13} N·mm$^{-3/2}$
m	3	3
initial crack depth a_i	0.1 mm	0.1 mm
initial crack length $2c$	5	5
final crack depth a_f	$0.99t_0$	$0.99t_0$

Table 8 Remaining fatigue life prediction of CFRHS K-joints

joint	SCF	DoB	fatigue life ($\times10^4$)
1	2.08	0.78	236.8
2	2.05	0.49	78.5

decrease of 66.85% in the fatigue life. The CFRHS K-joints with same *HSS*s, may have completely different fatigue lives due to the different *DoB*s.

6 Conclusions

The objective of this study was to improve the accuracy of fatigue assessment methods including the *S-N* curve method and fracture mechanics method for CFRHS K-joints, by considering the through-the-thickness stress characterized as *DoB*s. The FE model was developed and validated using the test result of a CFRHS truss. A database of *DoB*s was created and 190 numerical models were established under the balanced axial force, and four non-dimensional geometric parameters were evaluated. The parametric equation to predict *DoB*s of CFRHS K-joints was proposed through multiple regression analysis.

The main conclusions are as follows.

1) Compared with RHS joints, the σ_O, σ_I, and σ_M at CFRHS joints decreased, however, the value of the *DoB* increased, which indicated that the fatigue performance of RHS joints is improved after filling the chord with concrete.

2) The *DoB* values were positively associated with β and τ, and negatively related with 2γ. θ had little effect on the *DoB*.

3) An accurate evaluation of the proposed parametric equation showed that they matched well with the numerical results with R^2 being equal to 0.955, and the relative errors of DoB_P and DoB_R are less than 5%. In addition, the proposed parametric equation also satisfied the judgment criteria of DoE.

4) A reduction of 6.4% in *DoB* and 101.1% increase of *SCF* in CFRHS K-joints, was compared to CHS K-joints. Utilizing only *SCF* to evaluate the fatigue behavior without considering the influence of the *DoB* would cause errors.

5) To consider the influence of *DoB*, a correction factor was introduced to the *HSS S-N* curve, and the remaining life prediction process based on fracture mechanics for weld joints was presented.

6) A reduction of 37.17% was found in the *DoB*, resulting in a decrease of 66.85% in the fatigue life. The CFRHS K-joints with the same *HSS*s, may have completely different fatigue lives due to the different *DoB*s.

References

1. Han L H, Li W, Bjorhovde R. Developments and advanced applications of concrete-filled steel tubular (CFST) structures: Members. Journal of Constructional Steel Research, 2014, 100: 211−228

2. Huang H H, Chen K M, Wu Q X, Wang Q. Study on fatigue cracking of joint in a half-through CFST truss arch rib joint. Engineering Mechanics, 2017, 34: 167−173

3. Xu F, Chen J, Jin W L. Experimental investigation of SCF distribution for thin-walled concrete-filled CHS joints under the axial tension loading. Thin-walled Structures, 2015, 93: 149−157

4. Tong L W, Chen K P, Xu G W, Zhao X L. Formulae for hot-spot stress concentration factors of concrete-filled CHS T-joints based on experiments and FE analysis. Thin-walled Structures, 2019, 136: 113−128

5. Zheng J, Nakamura S, Okumatsu T, Nishikawa T. Formulation of stress concentration factors for concrete-filled steel tubular (CFST) K-joints under the three loading conditions without shear forces. Engineering Structures, 2019, 190: 90−100

6. Musa I A, Mashiri F R, Zhu X Q, Tong L. Experimental stress concentration factor in concrete-filled steel tubular T-joints. Journal of Constructional Steel Research, 2018, 150: 442−451

7. Kim I G, Chung C H, Shim C S, Kim Y J. Stress concentration factors of N-joints of concrete-filled tubes subjected to axial loads. International Journal of Steel Structures, 2014, 14(1): 1−11

8. Jiang L, Liu Y J, Fam A. Stress concentration factors in joints of square hollow section (SHS) brace and concrete-filled SHS chord under axial tension in brace. Thin-walled Structures, 2018, 132: 79−92

9. Jiang L, Liu Y J, Fam A. Stress concentration factors in concrete-filled square hollow section joints with perfobond ribs. Engineering Structures, 2019, 181: 165−180

10. Jiang L, Liu Y J, Fam A, Liu J, Liu B. Stress concentration factor parametric formulae for concrete-filled rectangular hollow section K-joints with perfobond ribs. Journal of Constructional Steel Research, 2019, 160: 579−597

11. Jiang L, Liu Y, Liu J, Liu B. Experimental and numerical analysis on the SCF of concrete-filled square hollow section Y-joints stiffened with perfobond ribs. Advances in Structural Engineering, 2020, 23(5): 869−883

12. Jiang L, Liu Y J, Fam A, Liu B, Long X. Fatigue behavior of integral built-up box Y-joints between concrete-filled chords with perfobond ribs and hollow brace. Journal of Structural Engineering, 2020, 146(3): 04019218

13. Jiang L, Liu Y J, Fam A, Wang K. Fatigue behavior of non-integral Y-joint of concrete-filled rectangular hollow section continuous chord stiffened with perfobond ribs. Engineering Structures, 2019, 191: 611−624

14. Li W, Cheng Y F, Wang D, Han L H, Zhao X L. Behavior of high-strength CFDST chord to CHS brace T-joint: Experiment. Engineering Structures, 2020, 219: 110780

15. Connolly M P M. A fracture mechanics approach to the fatigue assessment of tubular welded Y and K joints. Dissertation for the Doctoral Degree. London: University College London (University of London), 1987

16. Shen W, Choo Y S. Stress intensity factor for a tubular T-joint with grouted chord. Engineering Structures, 2012, 35: 37−47

17. Wei X, Wen Z, Xiao L, Wu C. Review of fatigue assessment approaches for tubular joints in CFST trusses. International Journal of Fatigue, 2018, 113: 43−53

18. Qian X, Jitpairod K, Marshall P, Swaddiwudhipong S, Ou Z, Zhang Y, Pradana M R. Fatigue and residual strength of concrete-filled tubular X-joints with full capacity welds. Journal of Constructional Steel Research, 2014, 100: 21−35

19. Chang E, Dover W D. Prediction of degree of bending in tubular X and DT joints. International Journal of Fatigue, 1999, 21(2): 147−161

20. Lee M M K, Bowness D. Estimation of stress intensity factor solutions for weld toe cracks in offshore tubular joints. International Journal of Fatigue, 2002, 24(8): 861−875

21. Berge S, Haswell J, Engesvik K. Fracture mechanics analysis of tubular joint tests degree of bending effects. In: International Conference on Offshore Mechanics and Arctic Engineering (OMAE-13). Houston: American Society of Mechanical Engineers, 1994

22. Ahmadi H, Lotfollahi-Yaghin M A, Asoodeh S. Degree of bending (DoB) in tubular K-joints of offshore structures subjected to in-plane bending (IPB) loads: Study of geometrical effects and parametric formulation. Ocean Engineering, 2015, 102: 105−116

23. Ahmadi H, Asoodeh S. Parametric study of geometrical effects on the degree of bending (DoB) in offshore tubular K-joints under out-of-plane bending loads. Applied Ocean Research, 2016, 58: 1−10

24. Ahmadi H, Zavvar E. Degree of bending (DoB) in offshore tubular KT-joints under the axial, in-plane bending (IPB), and out-of-plane bending (OPB) loads. Applied Ocean Research, 2020, 95: 102015

25. Nie F, Zhang Q, Qin X, Sun Y. Degrees of bending (DoBs) in buldge formed K-joints under balanced axial loads. Ocean Engineering, 2018, 166: 358−369

26. GB/T 228.1-2010. Metallic Materials-Tensile Testing-Part 1: Method of Test at Room Temperature. Beijing: General Administration of Quality Supervision, Inspection and Quarantine of the People's Republic of China, 2010 (in Chinese)

27. JTG D64-2015. Specifications for Design of Highway Steel Bridge. Beijing: General Administration of Quality Supervision, Inspection and Quarantine of the People's Republic of China, 2015 (in Chinese)

28. GB/T 50081-2002. Standard for Test Method of Mechanical Properties on Ordinary Concrete. Beijing: General Administration of Quality Supervision, Inspection and Quarantine of the People's Republic of China, 2002 (in Chinese)

29. JTG 3360-2018. Specifications for Design of Highway Reinforced Concrete and Prestressed Concrete Bridges and Culverts. Beijing: General Administration of Quality Supervision, Inspection and Quarantine of the People's Republic of China, 2018 (in Chinese)

30. GB 50661-2011. Chinese Standard the Welding Code for Steel Structure. Beijing: China Building Industry Press, 2018 (in Chinese)

31. XV-582-85. Recommended Fatigue Design Procedure for Welded Hollow Section Joints, Part 1 Hot Spot Stress Method for Nodal Joints. Strasburg: IIW Subcommission XV-E, 1985.

32. Ma Y, Liu Y, Wang K, Liu J, Zhang Z. Axial stiffness of concrete filled rectangular steel tubular (CFRST) truss joints. Journal of Constructional Steel Research, 2021, 184: 106820

33. Ma Y, Liu Y, Ma T, Zafimandimby M N H. Flexural stiffness of rectangular hollow section (RHS) trusses. Engineering Structures, 2021, 239: 112336

34. Morgan M R, Lee M M K. Prediction of stress concentrations and degrees of bending in axially loaded tubular K-Joints. Journal of Constructional Steel Research, 1998, 45(1): 67−97

35. Shao Y B, Lie S. Parametric equation of stress intehsity factor for tubular K-joint under balanced axial loads. International Journal of Fatigue, 2005, 27(6): 666−679

36. UK Department of Energy (DoE). Background Notes to the Fatigue Guidance of Offshore Tubular Joints. London: UK Department of Energy, 1983

37. Paris P, Erdogan F. A critical analysis of crack propagation laws. Journal of Basic Engineering, 1963, 85(4): 528−533

38. Aaghaakouchak A, Glinka G, Dharmavasan S. A load shedding model for fracture mechanics analysis of fatigue cracks in tubular joints. In: The 8th International Conference on Offshore Mechanics And Arctic Engineering. The Hague: British Maritime Technology, 1989